Patterns in the Bulk and at the Interface of Liquid Crystals

Ágnes Buka[1], Tamás Börzsönyi[1,2], Nándor Éber[1], and Tibor Tóth-Katona[1]

[1] Research Institute for Solid State Physics and Optics, Hungarian Academy of Sciences, H-1525 Budapest, P.O.Box 49, Hungary
[2] Groupe de Physique des Solides, CNRS UMR 75-88, Universités Paris VI et VII, Tour 23, 2 place Jussieu, 75251 Paris Cedex 05, France

1 Introduction

Liquid crystals (LCs) are substances possessing one or more mesophases between their liquid and solid phase. The sequence of these mesophases represents a step by step ordering of the structure. The nematic (N) phase is characterized by an orientational order of the elongated molecules described by the director $\mathbf{n}$, but the centers of mass of the molecules are arranged randomly. In the smectic (Sm) phases besides the orientational order the centers of mass of molecules form a layered structure. The smectic-A (SmA) phase has no positional order within the layers, while the smectic-B (SmB) phase is characterized by a long-range hexagonal order in each layer and by a weak correlation between the layers. The features of these and other LC phases are described in detail in the literature – see e.g. [1,2,3].

Liquid crystals are quite rich in pattern forming phenomena [4]. Owing to the orientational order LCs possess strongly anisotropic physical properties, which on the one hand result in the known pattern forming processes (observed in other systems such as Rayleigh-Bénard convection, viscous fingering, etc.) with richer scenarios, and on the other hand allow for new instability mechanisms (such as electrohydrodynamic convection, patterns at the Freedericksz transition, etc.). Furthermore, optical and other properties of LCs (e.g. birefringence, transparency, phase transition temperatures close to the room temperature, relatively fast transport processes) make the detection of patterns and realization of the experiment easier. Therefore LCs are often considered as model materials for studying both bulk and interfacial instabilities. In general, patterns in LCs are characterized by a relatively low threshold, high regularity and by a large aspect ratio (LC sandwich cells typically have lateral dimensions of $x, y \approx 1-2$ cm and thickness of $z \approx 10-100$ μm).

2 Bulk Instabilities

When a liquid crystal is confined between properly treated surfaces usually a homogeneous equilibrium (basic) state is obtained. In this state the elastic restoring torques force all spatially periodic director fluctuations to decay. External influences (electric or magnetic fields, thermal gradients or mechanical stresses) may,

D. Reguera, L.L. Bonilla, and J.M. Rubí (Eds.): LNP 567, pp. 298–318, 2001.
© Springer-Verlag Berlin Heidelberg 2001

however, lead to the appearance of destabilizing bulk torques. Then if the external field exceeds some critical threshold value the destabilizing torques may overcome the restoring ones, i.e. the amplitude of fluctuations starts growing and a nonhomogeneous pattern evolves. During this process typically a wavelength selection occurs, thus a pattern (stripes, spirals, targets, hexagons) is obtained which is characterized by a spatially periodic modulation of the director. The anisotropic optical properties of liquid crystals make these patterns easily observable either in microscopes with or without polarizers or via laser diffraction.

The above considerations are almost independent of the actual mechanism of the instability hence various physical processes, as e.g. the thermally driven Rayleigh-Bénard instability, the electric field induced convection or the shear flow instabilities, may provide very similar patterns [4].

2.1 Electroconvection

Electroconvection (electrohydrodynamic instability) [5] is a pattern forming process which – as explained by Carr and Helfrich in the late 60s – is related to the anisotropic physical properties of the liquid crystal.

In the classical electroconvection (EC) experiments a *planarly oriented* ($\mathbf{n} \| x$) layer of a nematic liquid crystal with negative dielectric anisotropy ($\varepsilon_a < 0$) corresponds to the homogeneous basic state. Besides the elastic torques due to the director gradient in this geometry the dielectric torques (which tend to keep the director perpendicular to the electric field) also serve as restoring torques. Due to the anisotropy of the electrical conductivity ($\sigma_a > 0$), however, in the presence of a director modulation (a thermal fluctuation) the electric currect may have a component perpendicular to the field which leads to charge separation. The electrostatic force acting on the charges induces a convective flow which provides a viscous destabilizing torque on the director.

Patterns at the Onset of the Electroconvection

The EC instability has been extensively studied since the first observation of a regular roll pattern, the Williams domains [6]. The formation of patterns is governed by two control parameters, the amplitude V and the frequency f of the applied voltage. Varying the frequency two regimes can be distinguished [5]. At low frequencies (in the 'conductive' regime) the periodic director and flow patterns are stationary and the charges oscillate with the field. At high frequencies (in the 'dielectric' regime) on the contrary, the charge distribution is stationary while the director and the flow velocities oscillate. The two regimes are separated by the cut-off frequency f_c which is roughly proportional to the electrical conductivity. In the 'conductive' regime there can be two different scenarios. The direction of the rolls is either perpendicular to the director (normal rolls, NR), or it is tilted (oblique rolls, OR) forming zig and zag domains. Oblique rolls can be observed at frequencies below the Lifshitz point f_L, with the roll angles increasing with decreasing frequency.

The threshold voltage V_c and the critical wavevector $\boldsymbol{q_c}$ of the roll pattern at the onset of the instability can be calculated by a linear stability analysis of the standard model of EC (a set of 6 coupled differential equations for the director, the flow velocity and the charge distribution) [7,5]. This model provides a full description of all above scenarios in agreement with the experiments.

In the 'conductive' regime V_c has a strong frequency dependence (it diverges approaching the cut-off frequency), while the wavelength λ_c of the rolls is about the sample thickness d. In the 'dielectric' regime the threshold grows with the square root of f, while the wavelength - only a few μm - is independent of the thickness and for typical cells ($d > 10$ μm) is much smaller than in the 'conductive' regime. In both regimes λ_c decreases with increasing frequency. One usually introduces $\epsilon = (V^2 - V_c^2)/V_c^2$ as a reduced control parameter characterising the deviation from the threshold.

Roll patterns can be observed in *twisted planar* cells too, where at the two boundaries the director is oriented perpendicular to one another. In this case the rolls are expected to be directed at 45 degrees (along the bisectrix of the preferred directions of the surfaces). This has been proved for the 'conductive' regime, however, according to recent experiments it might not always hold for 'dielectric' one. Diffraction measurements have shown a superposition of two roll structures above some critical frequency which depends on the sample thickness [8]. These rolls are oriented along the preferred orientations of the surfaces and are thus normal to one another. This observation indicates a possible transition from the standard bulk electroconvection state (rolls at 45^o) to an instability which is restricted to thin regions at the surfaces. Though such surface roll structures have been proposed earlier as a model for the 'dielectric' rolls [9], no theoretical explanation has yet been given for this transition which seems to occur at a small wavelength to thickness ratio.

In *homeotropic* cells ($\mathbf{n} \parallel z$) in electric field the first instability is a homogeneous tilt of the director (a Freedericksz transition – FT [1,3]), however, EC may set in at higher voltages. As the homeotropic orientation is fully degenerate in the surface plane, the direction of the tilt and hence that of the rolls are randomly selected and may vary in space and time. That represents a direct transition to spatio-temporal chaos already at the onset of the EC (soft mode turbulence) and is therefore subjected to detailed experimental and theoretical investigations [10,11,12,13,14].

The azimuthal degeneracy in the xy plane can be removed by an additional magnetic field $\boldsymbol{H}$ parallel to the surfaces (i.e. perpendicular to the electric field) which selects the tilt direction [11,13,15]. Under such conditions the EC scenarios typically are very similar to those in the planar case. It has been shown, however, both experimentally and theoretically that certain combination of the material parameters may lead to the appearance of a second (low frequency) Lifshitz point [16,17], i.e. to the preference of normal rolls at very low frequencies. For the time being this feature has only been observed in homeotropically oriented samples of Nematic Phase 5A (Merck).

Scenarios above Threshold

Until now we focused on the characteristics of the EC patterns at the onset of the instability. Increasing the voltage above V_c will, however, modify some of these characteristics (vary the wavevector or the director profile) and may also lead to new scenarios.

One of the scenarios at higher ϵ is the *'abnormal' roll* (AR) pattern which developes from normal rolls. As shown experimentally first in homeotropic [18,19], [15,16,17], later also in planar cells [20,21], in 'abnormal' rolls the director may rotate out of the tilt plane gaining a $\varphi \neq 0$ azimuthal angle, while the direction of the rolls remains unchanged. In homeotropic cells the appearance of such an out-of-plane component of the director leads to a net rotation of the optical axis of the sample, thus the 'abnormal' rolls can be easily detected using crossed polarizers (Fig. 1). In planar cells, however, due to the strong surface anchoring only a twist deformation can develop, thus detection requires more sophisticated techniques [22,21].

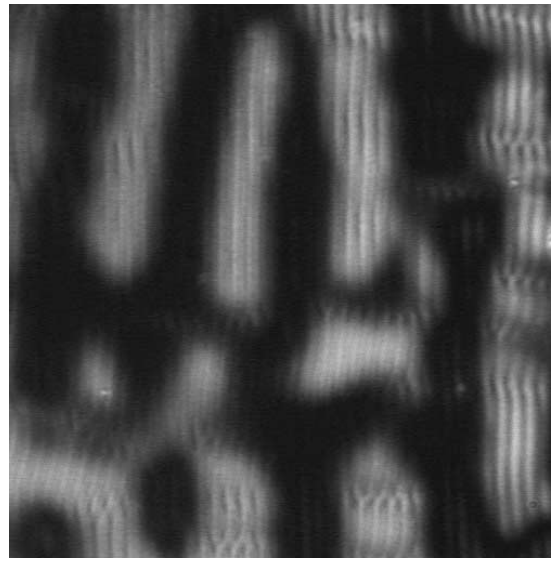

Fig. 1. 'Abnormal' roll domains (dark and bright patches) in a homeotropic nematic Phase 5A (Merck) in the presence of a small orienting magnetic field. Crossed polars are rotated by 8^o with respect to the magnetic field.

The equations of the standard model of EC are too complicated to be solved in the nonlinear regime. Instead, for a weakly nonlinear analysis a Ginzburg-Landau formalism is used, i.e. an amplitude equation is constructed [23,5]. Inspired by the experiments a reconsideration of the symmetries of the system has led to the realization of the fact that the pattern amplitude in itself is not enough to describe the nonlinear behaviour. Allowing for a Goldstone mode one has to

take into account an additional degree of freedom, the azimuthal angle φ of the director, which is coupled to the pattern amplitude A [24,20]. This feature is a consequence of the anisotropy of liquid crystals so it is not a privilege of EC, the coupling between A and φ is observable in thermal convection too [25]. Solving the resulting coupled differential equations thresholds of secondary instabilities could be derived and an $\epsilon - f$ phase diagram could be constructed. It showed that the NR pattern becomes unstable either due to a zig-zag instability (modulation of the roll direction) near the Lifshitz point or by a normal–'abnormal' roll transition at higher frequencies. In this latter case the out-of-plane component of the director appears as a forward (pitchfork) bifurcation for the azimuthal angle φ with increasing ϵ. As the rotations into both out-of-plane directions are equally probable, two types of domains with opposite sign of φ are expected to exist. The phase diagrams in the planar and the homeotropic (with a small superposed orienting magnetic field) geometry look similar except that in homeotropic samples the critical ϵ for the secondary instabilities are much smaller and the frequency range for the zig-zag instability is narrower. The theoretical predictions could be checked experimentally for both geometries and an excellent agreement has been found [21,16]. However, in contrast to the expectations, in homeotropic samples no distinct domains with sharp boundaries could be detected, instead a continuous (almost periodic) variation of φ could be observed with an approximate wavelength about 10 times that of the rolls [16,17] – 'prechevron' state (see later).

Increasing the voltage much above V_c the regularity of the roll pattern decreases by the appearance of *defects* which are typically dislocations in the convection roll pattern. The number of defects increases with the voltage as well as their mobility until we enter a chaotic, turbulent regime.

These defects play an important role as any adjustment of the wavevector can be realized only by generation and motion of defects. Changing the control parameters often leads to conditions where the actual wavevector $\mathbf{q}$ of the pattern is substantially different from the ideal $\mathbf{q_{id}}$ one belonging to the given voltage and frequency. If the wavevector mismatch $\mathbf{\Delta q} = \mathbf{q} - \mathbf{q_{id}}$ is large enough defects are usually generated in pairs and start moving to reduce $\mathbf{\Delta q}$. Motion of a defect along the roll direction ('climb') will modify the roll spacing, while motion normal to the rolls ('glide') can adjust their direction. Using the Ginzburg-Landau formalism the velocity $\mathbf{v}$ of an individual (far from and therefore not interacting with their neighbours) defect could be calculated yielding $\mathbf{v} \perp \mathbf{\Delta q}$ and a logarithmic singularity in v for $\Delta q \to 0$ [26]. In early experiments on planar EC only the 'climb' motion could be excited by sudden simultaneous change of the voltage and frequency [27,28]. In the homeotropic geometry the 'glide' motion can easily be generated by rotating the small orienting magnetic field. In recent experiments using local heating due to laser pulses for generating the defects both the predicted direction of $\mathbf{v}$ and the logarithmic singularity of $v(\Delta q)$ could be verified [17,29].

It has been known for a long time that in the high frequency EC (in the 'dielectric' regime) the regular roll pattern breaks down at higher voltages to

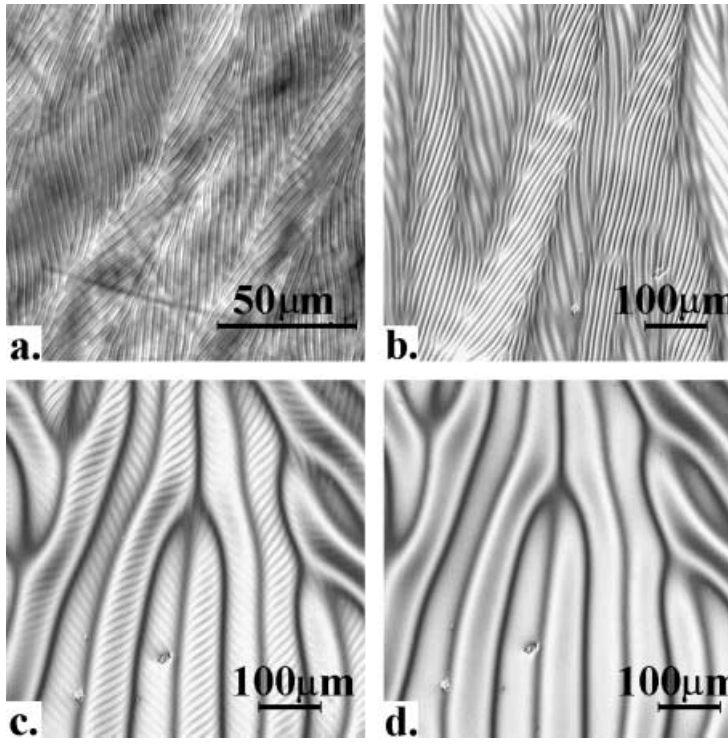

Fig. 2. Chevron scenarios in electroconvection of the homeotropic nematic Phase 5A (Merck) . a. 'dielectric' chevrons, b. 'conductive' defect mediated chevrons, c. 'conductive' defect free chevrons, d. prewavy pattern. Crossed polars. Sample thickness: a. $d = 20$ μm, b-d. $d = 60$ μm.

chevron scenario [30,31], i.e. to a periodic arrangement of domains. In the neighbouring domains the dielectric rolls are rotated alternatingly with respect to their initial direction (zig and zag chevron domains, Fig. 2a). It has been explored that the domain boundaries in these dielectric chevrons consist of an ordered chain of defects (dislocations) running along the initial roll direction [28,32,33], moreover, besides the rolls the orientation of the director is rotated too [22]. Thus in the chevron pattern the azimuthal angle φ of the director is periodically modulated which can be detected optically just as in the case of the 'abnormal' rolls in the 'conductive' regime. This φ modulation remains observable even if the visibility of the individual 'dielectric' rolls is much reduced either due to their small wavelength or to the bulk-surface transition mentioned earlier.

Recently the ordering of defects into chains has been theoretically explained [34]. It has been shown that its mechanism is not restricted to the 'dielectric' regime, under proper conditions similar chevrons can exist in the 'conductive' regime too. Such 'conductive' chevrons have actually been observed

in homeotropic cells, especially in the absence or with only a small orienting magnetic field (Fig. 2b) [15,17]. This scenario, which has been classified as a *defect mediated chevron* [35,36] reminding the role of defects, typically occurs at voltages much above the NR-AR transition.

Both the 'dielectric' and the 'conductive' chevrons possess a dual spatial periodicity, one for the convective ('dielectric' or 'conductive') rolls, the other for the defect chains. The wavelength of the latter is typically about an order of magnitude larger than that of the rolls, i.e. it can be larger than d.

These chevrons are not the only patterns with a wavelength larger than d. Such patterns have been reported for MBBA strongly doped with ionic dopants in planar and twisted planar ('wide' domains) [37,38,3], as well as in homeotropic geometries (*'prewavy' pattern*) [31,32,35,36]. These large wavelength patterns have in common that they evolve from a (seemingly) pattern free state at a threshold voltage having a weaker frequency dependence compared to either that of the 'conductive' or the 'dielectric' rolls. They can be observed with crossed polars (Fig. 2d), but the shadowgraph image with a single polarizer is almost invisible, in contrast to the usual convection rolls. That indicates an only azimuthal (without tilt) modulation of the director. It has been measured recently in homeotropic cells that the amplitude of the azimuthal modulation in the prewavy pattern increases with the voltage resembling a supercritical pitchfork bifurcation [36,39]. At higher voltages a transition to chevrons could be observed. However, while at higher frequencies these did correspond to the 'dielectric' chevrons mentioned above, near the Lifshitz point a different type of 'conductive' chevron pattern was observed (*defect free chevrons*) [35,36]. Though it looks similar to defect mediated chevrons, no defects (dislocations) are present, instead a continuos curvature of the rolls is observed (Fig. 2c). The chevron domains coincide with the stripes of the initial prewavy pattern. These defect free chevrons can thus be interpreted as 'conductive' normal rolls with azimuthally modulated director orientation.

The appearance of the 'wide domains' or the prewavy pattern has not been theoretically understood yet. At present no physical mechanism is known which could produce such a periodic static deformation (without flow) at thresholds lower than that of the electroconvection. The observed motion of dust particles in these patterns (and even at voltages below threshold) stress the importance of convection [40]. It suggests that an electroconvection mechanism, though different from the Carr-Helfrich one, might be responsible for the formation of these patterns [41]. One possibility could be the 'isotropic' mode [42] which is expected to produce very fine rolls unresolvable by the visible light, however, the chevrons formed from the defects of these fine rolls would possess similar features as the prewavy pattern. Unfortunately, no direct experimental evidence has been found to prove this assumption yet.

The defects (dislocations) mentioned so far usually possess a well defined core. Sometimes, however, one can observe *'long' defects*, where the core is delocalized to phase–jump lines extending over several rolls (Fig. 3a). Computer simulations

have shown that such structures are quite common in the AR range both in the planar and in the homeotropic geometry [43].

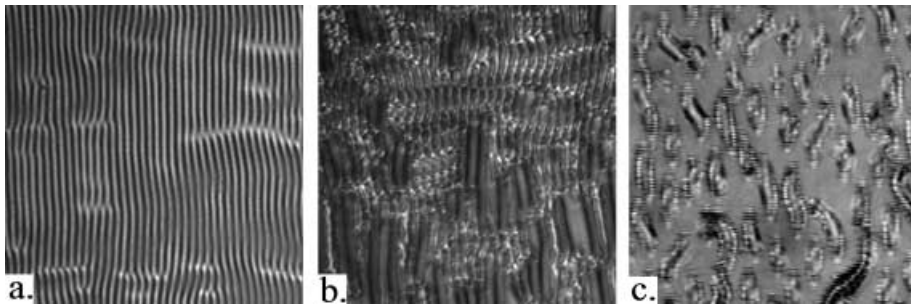

Fig. 3. Exotic patterns in electroconvection of nematics. a. 'long' defects and b. coexisting abnormal and CRAZY rolls in homeotropic Phase 5A (Merck), c. localized structures (worms) in planar 10E4.

Besides the defects in the convection rolls (dislocations, 'long' defects) the pattern may contain orientational singularities of the director field which usually appear in the form of domain walls or *disclination loops*. These orientational defects are quite common in homeotropic nematics. One recently reported example is the CRAZY roll pattern (Fig. 3b) [16,17] which may appear near the Lifshitz point above the normal-abnormal roll transition. The CRAZY rolls correspond to closed disclination loops located in the plane perpendicular to the cell surfaces and parallel to the rolls, which grow into the abnormal roll pattern without changing the wavelength or causing dislocations. Disclination loops play an important role in the Zvinger pattern [44] observed in a substance possessing a nematic-smectic phase transition as well as during the prewavy-wavy pattern transition. All these patterns appear high above threshold far beyond the applicability of either the linear or the weakly nonlinear stability analysis.

Another fascinating phenomenon in the nonlinear range is the spontaneous formation of localized states or pulses ('worms'). Chaotic localized traveling-wave states which coexist with the 'conduction' state, are long lived, appear and die at irregular locations and times, have unique small widths and irregularly varying length, as seen in I52 [45]. Time dependent localized states ('roll sinks' and 'butterflies') coexisting with the uniform state have been observed in 10E6 [46] (see an example on 10E4 in Fig. 3c).

2.2 Shear

Shear flow phenomena in nematic liquid crystals have drawn much attention to the experimental side, since the orientational instabilities are easy to be observed, and they take place at much smaller shear rates than the laminar-turbulent transition. This results from the fact, that the relaxation of the director fluctuations is usually orders of magnitude slower than that of the velocity fluctuations.

The basic feature of the instabilities is, that the flow (velocity) field $\mathbf{v}(r,t)$ and the director $\mathbf{n}(r,t)$ is coupled in the governing nemato-hydrodynamic equations. For most of the substances due to the orienting effect of the flow in the stationary case the director encloses a small angle Θ_{fl} with $\mathbf{v}$ (flow alignment) [1]. For some nematic liquid crystals (in particular near a nematic-smectic transition) no equilibrium state exists, but the flow exerts a continuous torque on the director, which might lead to a tumbling motion [47]. Here we will consider the case of flow aligning materials.

Rectilinear Flow

The instability mechanism varies considerably with the type of shear (stationary/oscillatory and Couette/Poiseuille flow), and each case has been considered both from the theoretical point of view and from the experimental side with a large variety of results which are summarized in [48] up to 1995.

The two basic cases are when the director is aligned (with external fields, or surface treatment) perpendicular to the shear plane (defined by $\mathbf{v}$ and $\nabla\mathbf{v}$) or in the shear plane. In the first case there is no torque on the director, but the configuration is unstable and above a threshold perturbations grow. The mechanism has been described by Pieranski and Guyon and was investigated in details [49]. In the second case the flow field exerts a torque on the director, and its orientation results in a balance between the elastic (or electric/magnetic) torques and the torque applied by the flow.

From now on we consider only the case of oscillatory flow fields (with the frequency f) that can be more easily realized experimentally than the case of stationary flow. One may first consider the response of the system before any instability occurs (basic state) where the director generally oscillates homogeneously around its initial equilibrium position. Beyond the small-amplitude linear regime one finds a response that is nonlinear in the shear strain. The temporal behavior of the director has been calculated using some approximations [50]. In the case of Couette flow (the shear is applied by moving one of the bounding plates in its plane) at low frequencies (f below about 400 Hz) the viscous penetration depth $\sqrt{\eta/\rho\omega}$ ($\omega = 2\pi f$), is much larger than the cell thickness d, where η is an appropriate effective shear viscosity and ρ denotes the mass density of the nematic. Then the flow can be approximated by the simple linear flow field, which amounts to neglecting the time derivative (inertia term) in the Navier-Stokes equation. With this assumption one may expect Freedericksz-type instabilities where the time-averaged director reorients homogeneously in the plane of the layer. For the simple linear Couette flow field no spatially homogeneous instabilities are predicted to occur (in contrast to the case of Poiseuille flow) [51,52], even if the possibility of transitions out of the flow plane is included.

Above a critical flow amplitude A_{xc}, transitions to spatially periodic roll states have been observed in homeotropic (director perpendicular to the confining plates) [53,54] and planar alignment [55]. In Fig. 4.a a developed roll pattern is shown in the homeotropic alignment [54].

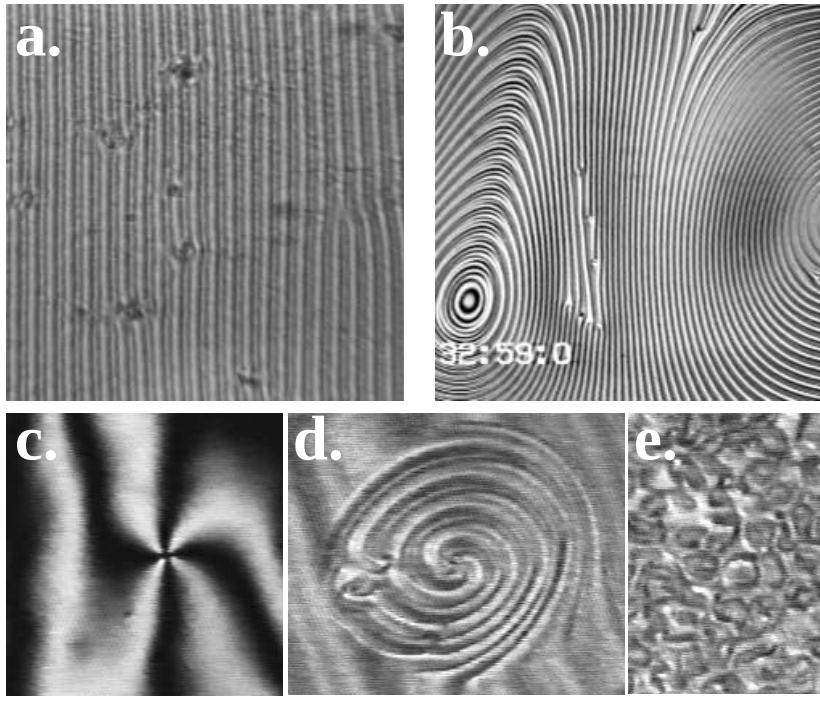

Fig. 4. **(a.)** *Rectilinear shear:* Roll pattern observed in polarized white light at $f = 80$ Hz and $A_x/d = 0.5$ in 5CB. The rolls are perpendicular to the direction of the upper plate oscillations. **(b.)** *Oscillatory compression of the sample:* A typical "target like" pattern in Phase 5 (Merck) at f=75 kHz for $d = 20$ μm. **(c-e.)** *Elliptic shear:* The spatio-temporal behavior of the system is considerably different in the three regimes: **(c.)** At large electric fields a nearly homogeneous precession is observed; **(d.)** Around $U = 1.2U_F$ spiral formation has been detected; **(e.)** At smaller voltages ($U < 1.2U_F$) spatiotemporal chaos can be observed. Phase 5 (Merck), f=155 Hz, $A_x = A_y = 3.4$ μm, and $d = 20$ μm.

The threshold amplitude of the roll pattern decreases with f [54]. A sufficiently rigorous linear stability analysis (that goes beyond the lowest-order modes) gives a good quantitative agreement with the experimental threshold values except for parameter ranges where the critical oscillation amplitude (in physical units) becomes large [54].

When comparing our data with the roll threshold obtained in the planar geometry [55] we find that the roll instability develops at smaller amplitudes in the homeotropic geometry than in the planar, as it is expected intuitively (the planar geometry is closer to the preferable flow alignment). However, the value of A_{xc} differs by a factor of 2, its frequency dependence is similar.

Director Precession, Phase Waves

An other interesting case is, when an elliptic shear is applied by the linear oscillation of the bounding plates in their plane perpendicular to each other. At large enough amplitudes and small ellipticities similar types of orientational instabilities take place as for the case of rectilinear flow. By increasing the ellipticity (towards the circular case) a transition from the roll regime to hexagonal patterns is observed [57].

An interesting configuration is, when the director is already tilted out by an external electric field from the initial homeotropic orientation ($\varepsilon_a < 0$), and a small amplitude elliptic shear is applied (below the instability threshold) [58,59]. The director is forced to precess around the z axis by the shear with a frequency Ω which is normally orders of magnitude smaller than f.

The value of Ω increases linearly with f and $A_x * A_y$ [59]. This observation is in accordance with the analytical calculations – which are done for low frequencies ($f < 10^4$ Hz), small amplitudes ($A/d \ll 1$), circular shear, and neglecting spatial dependence in the xy plane – yielding $\Omega \approx (\lambda/2)(A/d)^2\ 2\pi f$ where $\lambda = \alpha_3/\alpha_2 \approx 0.05$ for usual nematics.

The dependence of Ω on U is more complicated and for its understanding probably one has to take into account the spatial dependence. At sufficiently high voltages the director orientation varies slowly in space and precesses almost homogeneously in time (Fig.4.c). Around $1.2U_F$ inhomogeneities emit traveling waves and umbilics generate spiral waves (Fig.4.d), very similar to those observed in oscillatory and excitable chemical reactions [60]. At lower voltages one observes spatio-temporal chaos (Fig.4.e).

We have also performed experiments with linear mechanical vibration along z (compression) generated by piezo crystals ($f \approx 5$ - 100 kHz) attached to one of the bounding plates. The z oscillations presumably induce Poiseuille flow. As before, the slow precession occurred only in the Freedericksz distorted state.

Here the phase waves are typically emitted from certain locations in the form of target patterns (see Fig. 4.b), which presumably result from spatial inhomogeneities in the flow. The waves behave diffusively (even near U_F), which is probably due to the fact that at the high frequencies used the elastic contributions to the precession are irrelevant. In the immediate neighborhood of the FT and at not too high temperatures, a reversal of the precession was observed in Phase 5 and MBBA. For more details, see [61].

Director precession and phase waves have been observed previously in cells that were excited piezoelectrically at frequencies around 50 kHz [62]. The piezo crystal formed one of the bounding plates. Phenomena reminiscent of the phase waves were also seen in planar and homeotropic cells without electric field at frequencies 10 kHz $< f <$ 1 MHz [63]. There the waves originated from orientational defects at the surface.

3 Interfacial Instabilities

Interfacial instabilities appear at the interface that divides two different substances, phases or structures. The interface is driven by the gradient of a field which itself obeys a diffusion or Laplace equation. The emergence of the pattern results from the interplay between the stabilizing effect of the surface tension and interface kinetics and the destabilizing effect of the diffusive field.

From mathematical point of view these systems are similar. The surface tension causes curvature effects that should be incorporated into the equation describing a local equilibrium at the interface (moving boundary condition). Consequently, it is not surprising that all these systems show very similar patterns and that in the instability mechanisms the same parameters play important roles, i.e. the anisotropy of the surface tension and the interface kinetics.

Interfacial instabilities have been investigated extensively theoretically as well as experimentally in the last decades [64,65]. On the experimental side solidification [66], viscous fingering [67], electrochemical deposition [68], as well as growth of bacterial colonies [69] have been investigated. On the theoretical side mostly numerical approaches are used, since the analytical treatment of the problem is rather difficult except the stability analysis of the few (planar, circular or dendritic) solutions [65]. The two basic numerical methods are the sharp interface models (direct tracking of the front) [70,71] and the phase field models which are dynamic extensions of the Cahn-Hilliard theory of first-order phase transformations [72].

3.1 Propagation of a First Order Phase Transition Front

Here the growth is limited by diffusion (of heat or impurities) that exerts a destabilizing force on the (macroscopically) smooth interface. It is the surface tension and the phase transformation kinetics which tend to stabilize the interface against perturbations. Several liquid crystalline phase transitions are suitable to study the interfacial instability mechanisms:

The nucleation of the SmA phase in the isotropic (I) phase leads to the growth of battonets (rod like shape) and if they are bent the focal conic textures [2] develop. The formation of battonets is understood by taking into account the free energy difference between the two phases, the elastic energy and the surface energy [73].

The other well investigated phase transition is the $I \rightarrow$ columnar hexagonal transition [74,75]. In the columnar phase rod like objects (columns) are formed by the packing of disc like molecules on top of each other. A hexagonal order is present between the columns. The morphology diagram was reported and experimental results on both the surface tension and the kinetic anisotropy have been given [74].

Dendritic growth has been observed in the $I \rightarrow N$ [76] and $SmA \rightarrow SmB$ [77] phase transitions only in directional solidification.

In the smectic to crystal phase transition the morphological changes and the nature of mode selection were analyzed in [78].

Detailed studies have been made on the $N \rightarrow SmB$ transition [79,80,81,82,83] on a homologous series CCHm (m=3; 4; and 5) of a bicyclohexane compound. A thin (quasi 2D) sample after equilibration was cooled down below the phase transition temperature T_{NS} and the form of the nucleating and growing SmB domains was detected and analyzed as a function of the undercooling $\Delta T = T_{NS} - T$. Other details of the experimental setup can be found in [79]. With a proper experimental procedure both planar and homeotropic orientations have been achieved in the SmB and N phases and by that different anisotropies have been assured in the plane of observation.

Since the growth was observed in a quasi two-dimensional geometry, the angular dependence of the interfacial properties are relevant only in the plane of the sample.

As it can be expected, the anisotropies in a plane perpendicular to the smectic layers are much larger than parallel to them.

It has been shown [79,81], that in the case of a planar smectic germ **(A.)** the anisotropies resulted from the structure of the smectic phase are dominant in the pattern formation, while in the case of a homeotropic smectic germ **(B.)** the effects originating from the anisotropy of the nematic phase become comparable to the effects originating from the anisotropy of the smectic phase.

(A.) When the smectic layers are perpendicular to the sample (planar smectic germ) at low undercooling the formation of facets is observed that are parallel to the layers.

Normally the difference between the dynamics of a system with small anisotropies and a system showing facets can be summarized as follows. In a system with small anisotropies the solidification front is rough on the atomic level and the phase transformation (attachment of particles to the crystal) is limited by heat and impurity diffusion [65]. On the other hand faceted interfaces are smooth on an atomic scale and the growth of the solid phase is limited by the attachment kinetic process [84]. Thus in the later case usually the facet is blocked (does not advance) even at large undercoolings.

According to our observations this is not the case for the facets at the $N - SmB$ interface of CCH3, where even at very small undercoolings ($\Delta T = 0.02$ ^{o}C) the facet advances with a finite velocity. (The case of CCH4 and CCH5 is more complicated, here the propagation of the facet was only detectable at $\Delta T > 0.1$ ^{o}C which is still a small undercooling.)

Preliminary directional solidification measurements (a quasi-two-dimensional sample is pulled with a constant speed in a constant thermal gradient towards the cold side) also show that the nematic - smectic B front is more stable and variations in the facet velocity are much smaller than for traditional faceted fronts (e.g. the nematic - crystal interface of the same material) [85].

Phase-field simulations have shown [80], that even in the extreme (probably not realistic) case (i.e. supposing isotropic interfacial kinetics) with a "cusp-like" angular dependent surface tension obtained by the Wulff analysis of the nearly equilibrium shapes of the smectic-B domains, at small undercoolings the growth shapes are faceted (at a macroscopic scale) and at larger undercoolings

four-armed dendrites are formed, which is in accordance with our experimental observations [79].

(B.) To study the effect of the anisotropy of the nematic phase (liquid side) in the interfacial instabilities the most suitable configuration is when the smectic layers are parallel to the quasi two-dimensional layer of investigation, since the anisotropy of the SmB phase is the smallest in the plane of the smectic layers.

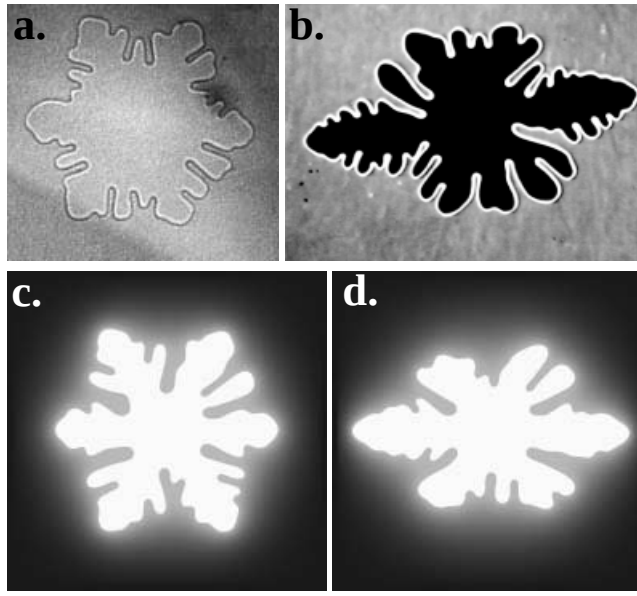

Fig. 5. The growth shapes of homeotropic smectic domains in homeotropic (**a.**), and in planar (**b.**) nematic phase at $\Delta T = 0.2\ ^o$C and $\Delta T = 0.15\ ^o$C respectively; Simulated growth shapes (using the phase field model) in isotropic (**c.**) and anisotropic (**d.**) liquid phase.

The growth morphologies have been compared for homeotropic and planar nematics [81] (see Fig. 5.a-b). Using the phase field model we have analyzed separately the effects coming from the superposing anisotropies of the surface tension, phase transformation kinetics and heat diffusion in the nematic phase.

The most interesting result is, that the heat diffusion anisotropy induces an elongation of the germ and the formation of dendritic tips perpendicular to the nematic director $\mathbf{n}$(N) [81] (See Fig. 5.a-b.).

This effect has also been observed in the case of planar smectic domains in CCH4 where the two opposite pairs of the main arms of the four-armed dendrites grow with slightly different velocities (asymmetric growth) if $\mathbf{n}$(N) is not a symmetry axis of the growth directions [82].

Finally, one should mention that material parameters of CCH3 (T_{NS}, volume change on phase transition, latent heat, electric conductivity, etc.) are in the

range that allows an easy control of the dendritic side-branching process by pressure oscillations or by a periodic heat release in the volume [83]. Such a method of controlling the side-branching process besides of academic aspects might have also implications in practical applications.

3.2 Viscous Fingering

The Saffman-Taylor (viscous fingering) problem, where a less viscous liquid (or gas) is pressed into a liquid with larger viscosity, represents a relatively simple case of nonlinear interfacial pattern formation and has been intensively studied – see e.g. reviews [86,67]. The evolution of the air – viscous fluid interface placed between two close parallel plates (Hele-Shaw cell) is determined by the pressure field p in the fluids satisfying the Laplace equation subjected to boundary conditions that are the pressures far from the interface on its both sides, and the pressure drop across the interface given by the Gibbs-Thomson condition and by the wetting properties.

For the interface of isotropic fluids experimental results agree well with the linear stability analysis [87,88]. Later stages of the interface growth in the radial geometry (after breakup of the initial circle) are less understood than those of the channel flow. For isotropic fluids the pattern continues to evolve through repeated tip-splitting to form more and more fingers.

Using non-Newtonian fluids (e.g. liquid crystal) as (usually) a more viscous fluid [89,90] however, gives a much richer morphological diagram than that obtained for isotropic fluids, due to the *inherent anisotropy*. As mentioned previously, in nematic liquid crystals the director field $\mathbf{n}$ and the velocity field $\mathbf{v}$ are coupled by nonlinear nematohydrodynamic equations – see e.g. [48,91] that in the lowest approximation lead to the same governing equations of viscous fingering as for isotropic fluids with some effective viscosity μ_{eff} and effective surface tension σ_{eff} [92,93].

For a $\mathbf{v} = v_x(z)$ velocity profile one has to distinguish different orientations of the nematic director which give different μ_{eff} as follows:

i. For planar cells and $\mathbf{n} \parallel x$ ($n_x \approx 1$, $n_y \ll 1$, $n_z \ll 1$): $\mu_{eff} = (\alpha_3+\alpha_4+\alpha_6)/2 = \eta_1$

ii. For homeotropic cells ($\mathbf{n} \parallel z$, i.e. $n_x \ll 1$, $n_y \ll 1$, $n_z \approx 1$): $\mu_{eff} = (\alpha_4 + \alpha_5 - \alpha_2)/2 = \eta_2$

iii. For planar cells and $\mathbf{n} \parallel y$ ($n_x \ll 1$, $n_y \approx 1$, $n_z \ll 1$): $\mu_{eff} = \alpha_4/2 = \eta_3$.

Here α_i ($i = 1-6$) are the Leslie viscosity coefficients and η_i ($i = 1, 2, 3$) are the Miezowitz viscosity coefficients (see e.g. [48]) that satisfy relation: $\eta_1 < \eta_3 < \eta_2$.

The orientation of the director with respect to the interface defines the surface tension of the air – nematic interface in the range of: $\sigma_\perp \leq \sigma_{eff} \leq \sigma_\parallel$, where $\sigma_\parallel$ and $\sigma_\perp$ are the surface tension parallel and perpendicular to $\mathbf{n}$, respectively. However, the change in the surface tension from $\sigma_\parallel$ to $\sigma_\perp$ is typically in the range of 20-50% for nematic substances [94], while the anisotropy in the viscosity is much larger: typically $\eta_2 \simeq 5\eta_1$ far below the nematic $\rightarrow$ isotropic phase transition temperature – see e.g. [95,96].

A number of experiments have been done in systems with a nematic liquid crystal as the more viscous fluid, for review see [67,92,93,97]. Four basic types of morphologies have been found in these systems: tip-splitting branches (SB), dense branching (DB), sparse dendritic (SD) and dense dendritic (DD) – see Fig. 6 [90,98]. The tip stabilization and the appearance of the dendritic pattern in a certain pressure – temperature range has been attributed to the anisotropy of μ_{eff} at the tip, induced by flow alignment of the nematic [88,99]. Recently, it has been shown by numerical simulation that non-Newtonian behavior can suppress tip splitting and produce dendritic growth with side-branches [100,101].

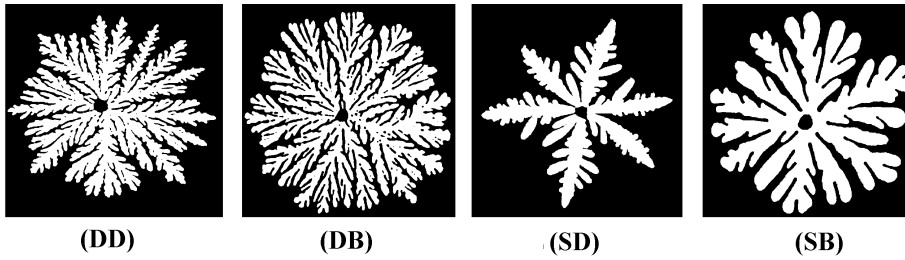

Fig. 6. Four basic morphologies of the air – 8CB liquid crystal interface.

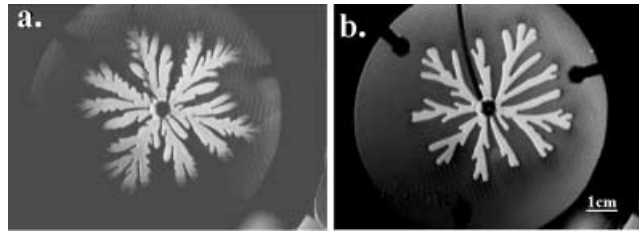

Fig. 7. Morphological transition at the nematic – air interface induced by electric field ($p_e = 123$ mbar); (a) $E = 0$, (b) $E = 0.5$ V/μm.

The effective viscosity μ_{eff} of the nematics and σ_{eff} of the N – air interface in the shear plane can be tuned by an electric field. Namely, using nematic liquid crystals with positive dielectric anisotropy $\varepsilon_a = \varepsilon_{\parallel} - \varepsilon_{\perp} > 0$ and applying an external electric field E perpendicular to the plane of the cell, one has two limiting cases: **(a)** When the shear torque [48] exerted on the director is much larger than the electric torque (high excess pressure p_e and low E, elastic torques are negligible in our case) the effective viscosity is $\mu_{eff} \approx \eta_1$ and the surface tension is $\sigma_{eff} \approx \sigma_{\parallel}$ (assuming 'flow alignment' so that $\mathbf{n}$ is in the plane of the cell and perpendicular to the interface). **(b)** In the opposite case, when the electric torque is much larger than the shear torque, we have $\mu_{eff} \approx \eta_2$ and

$\sigma_{eff} \approx \sigma_{\perp}$ (**n** is perpendicular to the bounding glass plates). Consequently, in the experiments μ_{eff} and σ_{eff} can be tuned depending on E and p_e in the range of: $\eta_1 \leq \mu_{eff} \leq \eta_2$ and $\sigma_{\perp} \leq \sigma_{eff} \leq \sigma_{\parallel}$ that can induce a morphological transition as it is shown in Fig. 7 [102].

Viscous fingering phenomena at the SmA – air interface are less well studied compared to the N – air system. Tip splitting of the fingers growing in the homeotropic SmA phase of 8CB has been observed leading to the dense-branching morphology (no anisotropy in the flow in the shear plane) with a decrease of the characteristic finger width with decreasing temperature [99]. In case of planar SmA phase (where anisotropy in the flow is present in the shear plane) however, a change in the direction of 'easy growth' of the fingers has been detected as a function of the excess pressure p_e [98] – a phenomenon that is still not fully understood.

Acknowledgement

We wish to thank S. Kai, L. Kramer, A. Krekhov, A. Hernández-Machado, J. Casademunt and R. Folch for discussions. Support of the Hungarian Research Grants No. OTKA-F022771, OTKA-T022772, OTKA-T031808 and the EU TMR Research Network 'Patterns, Noise and Chaos' is gratefully acknowledged. A.B. thanks the XVII Sitges Conference organizers for the invitation.

References

1. P. G. de Gennes and J. Prost: *The Physics of Liquid Crystals* (Clarendon Press, Oxford, 1993); S. Chandrasekhar, *Liquid Crystals* (Cambridge University Press, 1992)
2. G. Gray and J. Goodby: *Smectic Liquid Crystals* (Leonard Hill, Glasgow and London, 1984)
3. L. M. Blinov, V. G. Chigrinov: *Electrooptic Effects in Liquid Crystal Materials*, (Springer, Berlin, 1994).
4. Á. Buka, L. Kramer (Eds.): *Pattern Formation in Liquid Crystals*, (Springer, Berlin, 1995).
5. L. Kramer, W. Pesch: 'Electrohydrodynamic Instabilities in Nematic Liquid Crystals'. In: *Pattern Formation in Liquid Crystals*. ed. by Á. Buka, L. Kramer, (Springer, Berlin, 1995) pp. 221–255.
6. R. Williams: J. Chem. Phys. **39**, 384 (1963)
7. E. Bodenschatz, W. Zimmermann, L. Kramer: J. Phys. (France) **49**, 1875 (1988)
8. H. Bohatsch, R. Stannarius: Phys. Rev. E **60**, 5591 (1999)
9. S. Kai, K. Yamaguchi, K. Hirakawa: Jpn. J. Apl. Phys. **14**, 1653 (1975)
10. A. Hertrich, W. Decker, W. Pesch, L. Kramer: J. Phys. (France) II **2**, 1915 (1992); L. Kramer, A. Hertrich, W. Pesch: 'Electrohydrodynamic convection in nematics: the homeotropic case.' In: *Pattern Formation in Complex Dissipative Systems*. ed. by S. Kai. (World Scientific, Singapore, 1992).
11. S. Kai, K. Hayashi, Y. Hidaka: J. Phys. Chem. **100**, 19007 (1996)

12. Y. Hidaka, J.-H. Huh, K. Hayashi, S. Kai, M. I. Tribelsky: Phys. Rev. E **56**, R6256 (1997); Y. Hidaka, J.-H. Huh, K. Hayashi, M. I. Tribelsky, S. Kai: J. Phys. Soc. Jpn. **66**, 3329 (1997)
13. J.-H. Huh, Y. Hidaka, S. Kai: J. Phys. Soc. Jpn. **67**, 1948 (1998)
14. P. Tóth, Á. Buka, J. Peinke, L. Kramer: Phys. Rev. E **58**, 1983 (1998)
15. J.-H. Huh, Y. Hidaka, S. Kai: Mol. Cryst. Liq. Cryst. **328**, 497 (1999); J.-H. Huh, Y. Hidaka, S. Kai: J. Phys. Soc. Jpn. **68**, 1567 (1999)
16. A. G. Rossberg, N. Éber, Á. Buka, L. Kramer: Phys. Rev E **61**, R25 (2000); N. Éber, A. G. Rossberg, Á. Buka, L. Kramer: Mol. Cryst. Liq. Cryst. in press
17. Á. Buka, P. Tóth, N. Éber, L. Kramer: Phys. Reports, in press
18. H. Richter, Á. Buka, I. Rehberg: Mol. Cryst. Liq. Cryst. **251**, 181 (1994); H. Richter, Á. Buka, I. Rehberg: 'The Electrohydrodynamic Instability in a Homeotropically Aligned Nematic: Experimental Results'. In: *Spatio-Temporal Patterns*, ed. by P. E. Cladis, P. Palffy-Muhoray (Addison-Wesley, 1995) pp. 343–352
19. J.-H. Huh, Y. Hidaka, S. Kai: Phys. Rev. E **58**, 7355 (1998)
20. E. Plaut, W. Decker, A. G. Rossberg, L. Kramer, W. Pesch, A. Belaidi, R. Ribotta: Phys. Rev. Lett. **79**, 2367 (1997)
21. S. Rudroff, H. Zhao, L. Kramer, I. Rehberg: Phys. Rev. Lett. **81**, 4144 (1998); S. Rudroff, V. Frette, I. Rehberg: Phys. Rev. E **59**, 1814 (1999)
22. H. Amm, M. Grigutsch, R. Stannarius: Mol. Cryst. Liq. Cryst. **320** 11 (1998)
23. W. Pesch, L. Kramer: 'General Mathematical Description of Pattern-Formming Instabilities'. In: *Pattern Formation in Liquid Crystals*. ed. by Á. Buka, L. Kramer, (Springer, Berlin, 1995) pp. 69–90.
24. A. G. Rossberg, A. Hertich, L. Kramer, W. Pesch: Phys. Rev. Lett. **76**, 4729 (1996)
25. E. Plaut, R. Ribotta: Phys. Rev. E **56**, R2375 (1997)
26. E. Bodenschatz, W. Pesch, L. Kramer: Physica D **32**, 135 (1988); L. Kramer, E. Bodenschatz, W. Pesch: Comment in Phys. Rev. Lett. **64**, 2588 (1990)
27. S. Nasuno, S. Takeuchi, Y. Sawada: Phys. Rev. A **40**, 3457 (1989); S. Rasenat, V. Steinberg, I. Rehberg: Phys. Rev. A **42**, 5998 (1990)
28. S. Kai, N. Chizumi, M. Kohno: Phys. Rev. A **40**, 6554 (1989)
29. P. Tóth et al.: to be published
30. Orsay Liquid Crystal Group: Mol. Cryst. Liq. Cryst. **12**, 918 (1971)
31. K. Hirakawa, S. Kai: Mol. Cryst. Liq. Cryst. **40**, 261 (1977)
32. S. Kai, Y. Adachi, S. Nasuno: 'Stability Diagram, Defect Turbulence, and New Patterns in Electroconvection in Nematics'. In: *Spatio-Temporal Patterns*, ed. by P. E. Cladis, P. Palffy-Muhoray (Addison-Wesley, 1995) pp. 313–329
33. M. Scheuring, L. Kramer, J. Peinke: Phys. Rev. E **58**, 2018 (1998); H. Amm, R. Stannarius, A. G. Rossberg: Physica D **126** 171 (1999)
34. A. G. Rossberg, L. Kramer: Physica D **115**, 19 (1998)
35. J.-H. Huh, Y. Hidaka, A. G. Rossberg, S. Kai: Phys. Rev. E **61**, 2769 (2000)
36. J.-H. Huh: Electrohydrodynamic Instability and Nonlinear Dynamics in Liquid Crystals with Continuous Rotationaal Symmetry. Ph.D. Thesis. Kyushu University, Fukuoka, 2000
37. P. Petrescu, M. Giurgea: Phys. Lett. **59A**, 41 (1976); M. I. Barnik, L. M. Blinov, M. F. Grebenkin, A. N. Trufanov: Mol. Cryst. Liq. Cryst. **37** 47 (1976); L. Nasta, A. Lupu, M. Giurgea: Mol. Cryst. Liq. Cryst. **71**, 65 (1981)
38. A. N. Trufanov, L. M. Blinov, M. I. Barnik: 'A Novel Type of the Electrohydrodynamic Instability in Nematic Liquid Crystals'. In: *Advances in Liquid Crystal*

Research and Applications, ed. by L. Bata (Pergamon Press, Oxford - Akadémiai Kiadó, Budapest, 1980) pp. 549–560
39. J.-H. Huh, Y. Hidaka, S. Kai, Y. Yusril, N. Éber, T. Tóth-Katona, Á. Buka, to be published
40. R. Ribotta, G. Durand: J. Phys. (France) Coll. C3 **40** C3-334 (1979)
41. A. G. Rossberg: private communication
42. N. Felici: Rev. Gen. Electr. **78**, 717 (1969)
43. L. Kramer, H. Zhao, R. Benitez: private communication
44. C. Fradin, P. L. Finn, H. R. Brand, P. E. Cladis: Phys. Rev. Lett. **81**, 2902 (1998)
45. M. Dennin, G. Ahlers, D.S. Canell: Phys. Rev. Lett. **77**, 2475 (1996)
46. H.R. Brand, C. Fradin, P.L. Finn, W. Pesch, P.E. Cladis: Phys. Lett. A **235**, 508 (1997)
47. Ch. Gähwiller: Phys. Rev. Lett. **28**, 1554 (1972); P. Pieranski, E. Guyon: Comm. on Physics **1**, 45 (1976); M. Cohen, P. Pieranski, E. Guyon, C.D. Mitescu: Mol. Cryst. Lyq. Cryst. **38** 97 (1977); I. Zuniga, F.M. Leslie: Liq. Cryst.**5**, 725 (1989); Europhys. Lett. **9**, 689 (1989)
48. E. Dubois-Violette, P. Manneville: 'Flow Instabilities in Nematics'. In: *Pattern Formation in Liquid Crystals*, ed. by A. Buka, L. Kramer (Springer-Verlag, New York, 1996) pp. 91–163
49. P. Pieranski, E. Guyon: Solid State Comm. **13**, 435 (1973); Phys. Rev. A **9**, 404 (1974); P. Manneville, E. Dubois-Violette: J. Phys. **37**, 285 (1976)
50. M.G. Clark, F.C. Saunders, I.A. Shanks, F.M. Leslie: Mol. Cryst. Liq. Cryst. **70**, 195 (1981); W.R. Burghardt: J. Rheol. **35**, 49 (1991)
51. A.P. Krekhov, L. Kramer, Á. Buka, A.N. Chuvyrov: J. Phys. II (France) **3**, 1387 (1993)
52. A.P. Krekhov and L. Kramer: J. Phys. II (France) **4**, 677 (1994); Phys. Rev. E **53**, 4925 (1996)
53. F. Scudieri: J. Appl. Phys.**49**, 1289 (1978); E. Guazzelli: Thèse de 3me cycle. Université Paris-Sud, Orsay, 1981
54. T. Börzsönyi, A.P. Krekhov, Á. Buka, L. Kramer: Phys. Rev. E **58**, 7419 (1998)
55. S.J. Hogan, T. Mullin, P. Woodford: Proc. R. Soc. London, Ser.A **441**, 559 (1993); R. Linsey, S. Hogan: Preprint (1996).
56. E.N. Kozhevnikov: Zh. Eksp. Teor. Fiz. **91**, 1346 (1986); Sov. Phys. JETP **64**, 793 (1986)
57. P. Pieranski, E. Guyon: Phys. Rev. Lett. **39**, 1281 (1977); E. Guazzelli, E. Guyon: J. Phys. (France) **43**, 985 (1982); E. Guazzelli: In: *Nematics, NATO ASI Vol.332*. Kuwer, Dordrecht, 1991; E. Guazzelli, G. Dewel, P. Borckmans, D. Walgraef: Physica D **35**, 220 (1989); E. Dubois-Violette, F. Rothen: J. Phys. (France) **39**, 1039 (1978)
58. J.-M. Dreyfus, P. Pieranski: J. Phys. (France) **42**, 459 (1981).
59. T. Börzsönyi, Á. Buka, A.P. Krekhov, O.A. Scaldin, L. Kramer: Phys. Rev. Lett. **84**, 1934 (2000)
60. A. de Wit, Adv. Chem. Physics, ed. by: I. Prigogine, S.A. Rice (John-Wiley, New York, 1999) Vol.109, p. 435.
61. T. Börzsönyi, Ph.D. dissertation, Budapest, 1998 (in English).
62. A. N. Chuvyrov: Zh. Eksp. Teor. Fiz. **82**, 761 (1982) [Sov. Phys. JETP **55**, 451 (1982); A.N. Chuvyrov, O.A. Scaldin, V.A. Delev: Mol. Cryst. Liq. Cryst.**215**, 187 (1992).
63. F. Scudieri: Ann. Phys.**3**, 311 (1978).
64. *Solids far from equilibrium*. Ed. by C. Godrèche (Cambridge University Press, Cambridge, 1992)

65. J. Langer: Rev. Mode. Phys. **52**, 1 (1980)
66. E. Rubinstein, M. Glicksman: J. of Crystal Growth **112**, 97 (1991); K. Koo, R. Ananth, W. Gill: Phys. Rev. A **44**, 3782 (1991); M. Muschol, D. Liu, H. Cummins: Phys.Rev. A **46**, 1038 (1992); M. Glicksmann, N. Singh: J. Cryst. Growth **98**, 277 (1989); A. Dougherty, J. Gollub: Phys. Rev. A **38**, 3043 (1988)
67. K. McCloud, J. Maher: Phys. Rep. **260**, 139 (1995)
68. D. Grier, E. Ben-Jacob, R. Clarke, L. Sander: Phys. Rev. Lett. **56**, 1264 (1986); D. Barkey, F. Oberholtzer, Q. Wu: Phys. Rev. Lett. **75**, 2980 (1995)
69. E. Ben-Jacob, O. Shochet, A. Tenenbaum, I. Cohen, A. Czirok, T. Vicsek: Fractals **2**, 15 (1994)
70. O. Shochet, K. Kassner, E. Ben-Jacob, S. Lipson, H. Müller-Krumbhaar: Physica A **181**, 136 (1992)
71. H. Müller-Krumbhaar: 'Theory of dendritic crystal growth'. In: *Morphology of crystals* ed. by: I. Sunagawa (Terra Scientific Publishing Company, Tokyo, 1987)
72. O. Penrose, P. C. Fife: Physica D **43**, 44 (1990); S.-L. Wang, R. F. Sekerka, A. A. Wheeler, B. T. Murray, S. R. Coriell, R. J. Braun, G. B. McFadden: Physica D **69**, 189 (1993); A. Karma, W. J. Rappel: Phys. Rev. E **57**, 4323 (1998); R. Kobayashi: Physica D **63**, 410 (1993)
73. R. Pratibha, N. Madhusudana: J. Phys. II. (France) **2**, 383 (1992); H. Naito, M. Okuda, O.-Y. Zhong-can: Phys. Rev. Lett. **70**, 2912 (1993)
74. P. Oswald, J. Malthéte, P. Pelcé: J. Phys. **50**, 2121 (1989); J. Géminard, P. Oswald, D. Temkin, J. Malthête: Europhys.Lett. **22**, 69 (1993)
75. P. Oswald: J. Phys. (France) **49**, 2119 (1988); P. Oswald: J. Phys. (France) **49**, 1083 (1988); J. Géminard, P. Oswald: J. Phys. II (France) **4**, 959 (1994)
76. P. Oswald, J. Bechhoefer, A. Libchaber: Phys. Rev. Lett. **58**, 2318 (1987)
77. J. Bechhoefer, P. Oswald, A. Libhaber, C. Germain: Phys.Rev. A **37**, 1691 (1988)
78. J. Hutter, J. Bechhoefer: Physica A **239**, 103 (1997)
79. T. Tóth Katona, T. Börzsönyi, Z. Váradi, J. Szabon, Á. Buka, R. González-Cinca, L. Ramírez-Piscina, J. Casademunt, A. Hernández-Machado: Phys. Rev. E. **54**, 1574-1583 (1996)
80. R. González-Cinca, L. Ramírez-Piscina, J. Casademunt, A. Hernández-Machado, L. Kramer, T. Tóth Katona, T. Börzsönyi, Á. Buka: Physica D **99**, 359 (1996)
81. T. Börzsönyi, Á. Buka, L. Kramer: Phys. Rev. E **58**, 6236 (1998)
82. R. González-Cinca, L. Ramírez-Piscina, J. Casademunt, A.Hernández-Machado, T. Tóth Katona, T. Börzsönyi, Á. Buka: J. Cryst. Growth **193**, 712 (1998)
83. T. Börzsönyi, T. Tóth-Katona , Á. Buka, L. Gránásy: Phys. Rev. Lett. **83**, 2853 (1999); T. Börzsönyi, T. Tóth-Katona , Á. Buka, L. Gránásy: Phys. Rev. E **62**(September 2000)
84. A.A. Chernov: Contemporary Physics **30**, 251 (1989); W.K. Burton, N. Cabrera, F.C. Franck: Phil. Trans. Roy. Soc. London **2431**, 40 (1951)
85. T. Börzsönyi, S. Akamatsu G. Faivre: To be published.
86. D. Bensimon, L. Kadanoff, S. Liang, B. Shraiman, C. Tang: Rev. Mod. Phys. **58**, 977 (1986)
87. L. Paterson: J. Fluid Mech. **113**, 513 (1981)
88. Á. Buka, P. Palffy-Muhoray: Phys. Rev. A **36**, 1527 (1987)
89. K. Makino, M. Kawaguchi, K. Aoyama, T. Kato: Phys. Fluids **7**, 455 (1995); M. Kawaguchi, K. Makino, T. Kato: Physica A **246**, 385 (1997)
90. Á. Buka, J. Kertész, T. Vicsek: Nature **323**, 424 (1986)
91. H. Pleiner, H. Brand: 'Hydrodynamics and Electrohydrodynamics of Liquid Crystals'. In: *Pattern Formation in Liquid Crystals*, ed. by Á. Buka, L. Kramer (Springer-Verlag, New York, 1996) pp. 15–67

92. L. Lam, H. Morris, R. Shao, S. Yang, Z. Liang, S. Zheng, H. Liu: Liq. Cryst. **5**, 1813 (1989)
93. Á. Buka: 'Viscous Fingering in Liquid Crystals'. In: *Pattern Formation in Liquid Crystals*, ed. by Á. Buka, L. Kramer (Springer-Verlag, New York, 1996) pp.291–305
94. V. Tsvetkov, O. Tsvetkov, V. Balandin: Mol. Cryst. Liq. Cryst. **329**, 305 (1999)
95. H. Kelker, R. Hatz: *Handbook of Liquid Crystals*. (Verlag Chemie, Weinheim 1980)
96. C. Gähwiller: Mol. Cryst. Liq. Cryst. **20**, 301 (1973)
97. A. Sonin: Rivista del Nuovo Cimento **14**, 1 (1991)
98. Á. Buka, P. Palffy-Muhoray: J. Phys. (France) **49**, 1319 (1988)
99. Á. Buka, P. Palffy-Muhoray, Z. Rácz: Phys. Rev. A **36**, 3984 (1987)
100. K. Kondic, M. Shelley, P. Palffy-Muhoray: Phys. Rev. Lett. **80**, 1433 (1998)
101. R. Folch, J. Casademunt, A. Hernández-Machado: Phys. Rev. E **61**, 6632 (2000)
102. R. Folch, T. Tóth-Katona, Á. Buka, J. Casademunt, A. Hernández-Machado: To be published